

Flow Control of Dispersion Section of Hydraulic Headbox of Papermaking Machine

Sumida, M.^{1,*} and Suzuki, S.²

¹Faculty of Engineering, Kinki University

¹¹ Takaya Umenobe, Higashi-Hiroshima, Hiroshima 739-2116, Japan

²Metso Paper Japan Co., Ltd., 3-10 Togiya-cho, Okayama 700-0826, Japan

Email: setsuo.suzuki@metso.com

Received date 2nd August 2011; Accepted date 26th November 2012

ABSTRACT

An experimental study of the flow in a modeled hydraulic headbox of a papermaking machine was performed. The turbulent boundary layer generated on the partition plates in the dispersion part and the wake formed downstream of the plates were investigated by a flow visualization technique using the smoke-wire method and by hot-wire measurement. Control of the flow characteristics was examined for various combinations of two types of channel and four types of inserted plate that differ in convergence and trailing-edge shape, respectively. As a result, rectification by the use of a convergent channel was found to be effective in realizing a uniform time-averaged velocity distribution and in reducing and unifying the turbulence intensity. Furthermore, the trailing edges with tapered and wavy shapes were effective for obtaining a uniform time-averaged velocity distribution, and the tapered edge was highly effective for making the turbulence intensity a uniform distribution.

Key Words: Flow Control, Flow Visualization, Wake, Convergent Channel, Turbulence, Headbox, Papermaking Machine

1. INTRODUCTION

The purpose of this study is to investigate the flow field from the dispersion section to the rectification section of a modeled hydraulic headbox of a papermaking machine. To this end, we carry out a visualization experiment and velocity measurement on the turbulent boundary layer generated on a partition plate and on the wake formed downstream of the plate. We examine the flow characteristics for plates with trailing edges of various shapes inserted in two types of channel and study their control. First of all, to illustrate the types of flow under investigation, we show a photograph of pulp fibers and the state of a pulp suspension flowing in a duct in Figs. 1 and 2, respectively.

In recent years, our highly advanced information-based society has invented many types of equipment associated with office automation. For example, the diversification of paper products used for printers is now under way. On the other hand, the highly effective use and recycling of paper resources are required simultaneously. Energy saving is also an aim in paper manufacturing. Hence, the demand for high-performance papermaking machines is expected to further increase. With this background, effort has been made from various viewpoints [1–6] to improve the quality of paper along with the speed of machines used to manufacture paper.

A papermaking machine consists of five parts: a headbox, a wire, a press, a dryer, and a calender and reel, as shown in Fig. 3. The headbox, from which pulp suspension is jetted out, is the most important part for papermaking. It controls the flocculation of pulp fibers and jets out pulp liquid containing pulp fibers with as uniform concentration as possible (see Figs. 1 and 2). Many modifications have been

*Corresponding author, Email: sumida@hiro.kindai.ac.jp

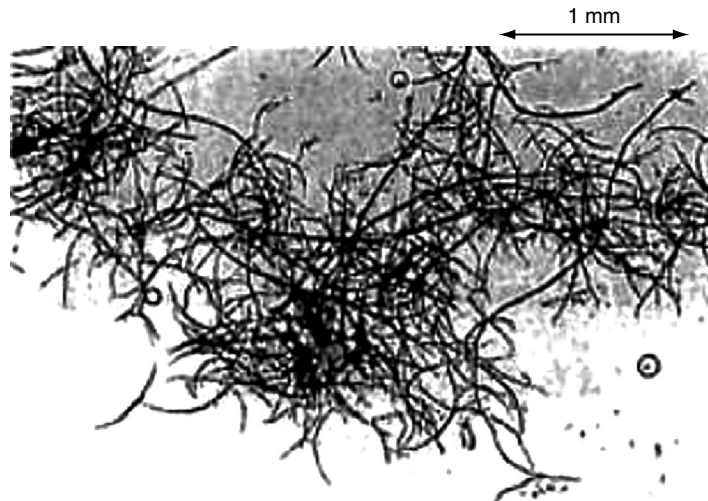


Figure 1. Photograph of pulp fibers.

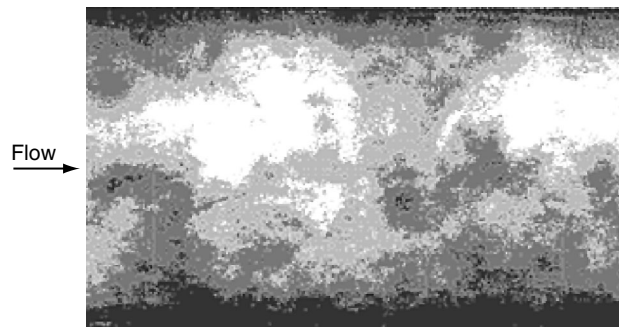


Figure 2. State of pulp suspension flowing in a duct.

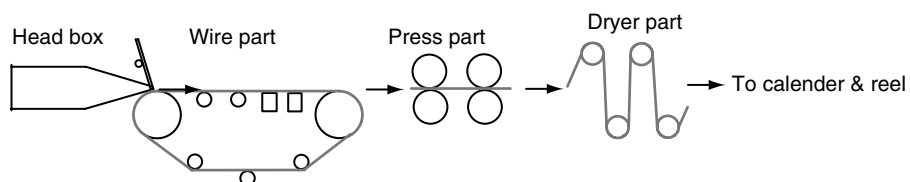


Figure 3. Schematic diagram of components of papermaking machine.

made to papermaking machines to rectify the raw material discharged from the pump in the headbox and to uniformly divide it in the width direction. Thus, the structure of the headbox has undergone many changes [1, 2].

A hydraulic headbox contains distributors and partition plates, as shown in Fig. 4. The distributors allocate the pulp liquid in the width direction. Subsequently, the pulp liquid is distributed by the partition plates inserted in the channel and is rectified through the passages in the headbox. In this way, the pulp liquid not only ensures the uniformity of the fiber dispersion but also makes the fiber orientation uniform. The aim of this work is to find suitable combinations of the channel and trailing edge of the partition plates that result in uniform velocity profiles and in reducing the turbulence intensity in the wake flow of the partition plates in the headbox. It was found in previous works (see below) that it is important for the dispersion part of the headbox to inhibit the following flow states as much as possible: 1) longitudinal vortices are induced in the boundary layer on the partition plates;

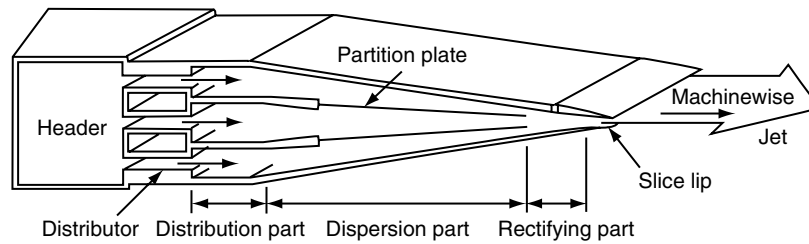


Figure 4. Structure of hydraulic headbox.

2) a Karman's vortex is formed behind the plates; and 3) factors creating disturbance such as longitudinal vortices are generated in the wake. Moreover, it is necessary to create flow conditions under which the amplitude of the surface waves produced and the scatter of the pulp liquid jetted out on the wire part are minimized. In addition, it is also necessary to inhibit the flocculation of pulp fibers and the generation of streaks to manufacture paper with a consistent texture. To comply with the above requirements, one must first clarify the flow characteristics of the boundary layer on the partition plates and in the wake behind the plates. Thus, the realization of methods of clarifying and controlling such characteristics is expected to be the key to optimizing the design of the headbox.

Although numerous attempts have been made, it is not easy to improve the fiber dispersion and simultaneously to obtain a uniform velocity distribution. Hence, there are few researches. For example, Carlsson et al. [7] reported experimental results for the fiber orientation in a laboratory-scale headbox, in which images of fibers very close to the wall of the headbox contraction were captured. Unfortunately, the wake flow of a partition plate was not observed owing to measurement difficulties in the experiment. Another study [8] focused on optimizing the contraction angle to obtain a uniform velocity distribution of the zero-concentration pulp liquid (water) in a header without a partition plate. Subsequently, Olson et al. [9] proposed a model to predict the fiber orientation distribution in a planar contraction. Furthermore, Hämäläinen and Makinen [10] used numerical analysis to consider the problem of controlling the fiber orientation distribution at the end of a contraction by varying its shape. However, these studies did not consider the effect of the shape of the planar contraction on the flow. Thus, the wake flow of the inserted partition plates was not a subject of the investigations.

The dispersion and jetting-out parts in the headbox are modeled as a flow field in which the flow along the inserted plate is accelerated owing to the contraction of the passages from the vicinity of the trailing edge. There have been many fundamental studies on this flow problem. For example, the flow along a flat plate was discussed in detail by Tani [11]. For the wake near the trailing edge, Toyoda and Hirayama [12] studied the transition process from the turbulent boundary layer before the trailing edge to its wake. Furthermore, for the wake in the contraction, various researchers [13–17] have investigated a two-dimensional wake under a pressure gradient. Prabhu and Narasimha [13] studied a wake flow with a small velocity defect for relatively long distances downstream of the trailing edge. In reference [14], on the other hand, the flow just behind a simple trailing edge was considered. Liu and co-workers [15, 16] conducted measurements of a wake flow generated by a plate with a tapered trailing edge and investigated the effects of imposed pressure gradients on the turbulent flow. Moreover, Parsheh and Dahlkild [17] analytically and experimentally studied the wakes of both tapered and blunt edges, in which the plate is sufficiently long to reach the outlet of a planar contraction. They also focused on the evolution and relaminarization of a turbulent wake in a strong pressure gradient. Because the above studies are fragmentary from the viewpoint of obtaining useful information for optimizing the passages in the dispersion part of the headbox, it is necessary to obtain basic information on the flow characteristics in the headbox to improve its performance.

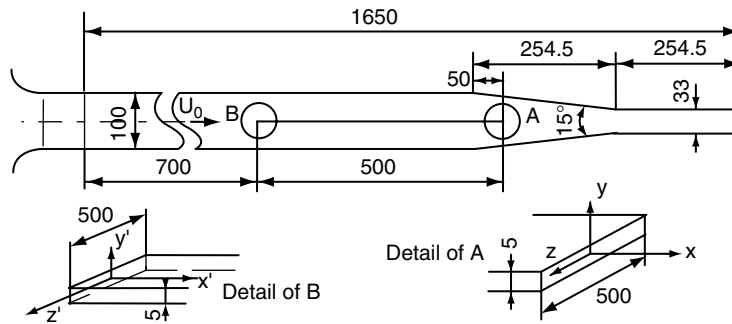
In this paper, considering the above circumstances, we deal with the flow problem of a wake downstream of a partition plate with several trailing-edge shapes inserted in both linearly and smoothly convergent channels. The flows were visualized by the smoke-wire method, and velocity measurement was performed with a hot-wire anemometer. The results obtained for the flow characteristics are expected to contribute to improving the headbox.

2. EXPERIMENTAL APPARATUS AND PROCEDURES

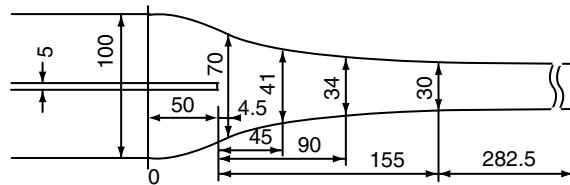
2.1. Experimental Apparatus

A schematic diagram of the channels employed in this experiment and the geometry of the partition plates inserted in them are shown in Figs. 5 and 6, respectively. The dimensions were based on those of a practical papermaking machine, that is, the dimensions were about three times larger in the actual machine. The partition plates were made of transparent acrylic. The width of the passages was 500 mm. A suction-type apparatus was used in the experiment, in which the right end of the channels was connected to a blower controlled by an inverter. Moreover, to examine the effect of channel convergence on the flow characteristics of the wake behind the inserted plate, a similar experiment was performed on a parallel channel. The length and thickness of the plates were 500 and 5 mm, respectively.

Four trailing-edge shapes, as shown in Fig. 6, were employed to investigate the relationships between the fiber dispersion and the turbulence and vortex structure of the wake. For the rectangular shape in Fig. 6(a), a separated shear layer is formed. For the R-cut shape in Fig. 6(b), it is considered that longitudinal vortices occur with greater ease than for the rectangular shape. Furthermore, the plate with a taper angle of about 1.4° in Fig. 6(c) corresponds to that employed in an actual headbox. On the other hand, for the wavy shape in Fig. 6(d), three-dimensional longitudinal vortex streets are induced, implying that this shape promotes the diffusion of the wake.



(a) Linearly convergent channel



(b) Smoothly convergent channel

Figure 5. Test channels (side view, unit mm).

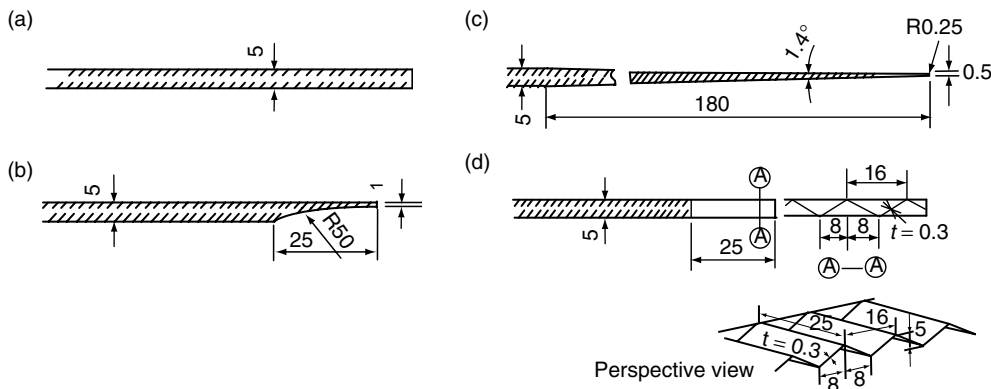


Figure 6. Configurations of trailing edge of partition plate (unit mm). (a) Rectangular shape, (b) R-cut shape, (c) Tapered shape, (d) Wavy shape.

The coordinate system used in this study is shown in Fig. 5(a). The origin of the coordinates is the center of the trailing edge of the plate. The x -axis is in the stream direction, the y -axis is perpendicular to the stream and plate directions, and the z -axis is in the spanwise direction. In addition, we use the x' -axis to represent the distance measured along the stream from the leading edge of the plate for convenience.

In a practical headbox, the pulp liquid at the entrance flows with a turbulence of 3–5%. Hence, it is considered that the boundary layer flow on the inserted plate is in the turbulent state from the vicinity of its leading edge. On account of this, in the present experiments, a 200-mesh wire net was installed behind the bell mouth at the entrance of the channel, thereby forcibly generating a turbulence of about 1% in the primary flow. Furthermore, the leading edge of each plate was cut off perpendicularly to the x' -axis to promote the transition of the boundary layer to a turbulent flow. The thickness of the plate was $d = 5$ mm and the cross-sectional average velocity at the entrance was $U_0 = 3$ m/s. These values give a Reynolds number ($U_0 d/\nu$) of 940, with ν being the kinematic viscosity of air. Under these conditions, the flow separated at the leading edge reattaches to the plate at a distance of about $5d$ further downstream [18]. Thereafter, the boundary layer develops into a turbulent boundary layer. When we roughly estimate the flow in terms of the Reynolds number defined by $U_e \theta/\nu$, the value at $x' = 400$ mm becomes about 300. Here, θ and U_e are the momentum thickness of the boundary layer and the velocity of the primary flow, respectively, at position x' . Thus, the boundary layer near the trailing edge of the plate can be considered to be in a nearly fully developed turbulent state [19]. (Please refer to Fig. 8, which will be described later).

From the above discussions, $x' = 450$ mm ($x = -50$ mm) was chosen as the point where the channel starts to converge. Moreover, the flow in the region downstream of $x' = 300$ mm was measured.

2.2. Flow Visualization and Velocity Measurement

The flow was visualized by the smoke-wire method. We used a stainless-steel wire of 0.1 mm diameter, to which oil containing silver powder was added. The fluid layers to be rendered visible were illuminated with sheet light of 8 mm thickness from 3–6 stroboscopes, onto which a wide adaptor was mounted. The boundary layer on the plate and the wake were visualized. The flows in the vertical, horizontal and cross-sectional planes parallel to the x - y , x - z and y - z planes, respectively, were photographed with a Nikon FE2 camera at a shutter speed of 1/60 s. To increase lighting effects, a matt black coating was applied on the inside of the test channels except on the slit windows.

The velocity was measured using a constant-temperature hot-wire anemometer (KANOMAX, System 7112) with a temperature compensation circuit. An I-type probe with a tungsten wire of 5 μ m diameter and 1 mm active length was used. The probe was calibrated using a 1960 mm² circular nozzle. The temperature of the working and ambient air was kept at $30 \pm 1^\circ\text{C}$ while measuring the velocity. Thus, the discrepancy in the velocity-voltage calibration curve before and after measurement was 1.5% or less. Figure 7 shows the measurement locations and the setup of the hot-wire probe. The probe was mounted on a traversing device controlled by a personal computer and was aligned at a prescribed position with an

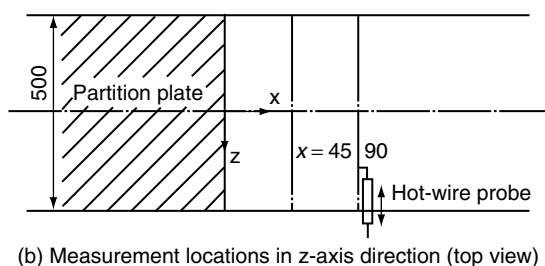
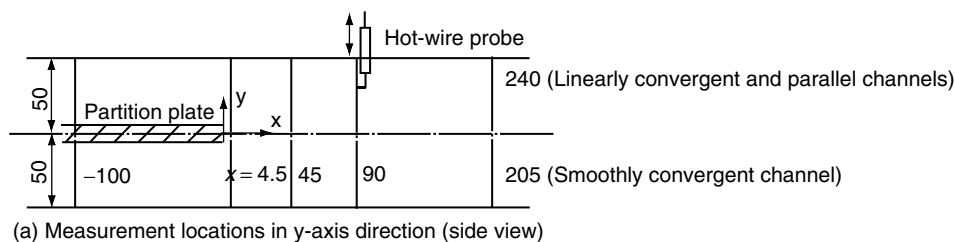


Figure 7. Measurement locations and probe set (unit mm).

accuracy within 0.05 mm. The time average U and turbulence intensity u_{rms} of the velocity u in the stream direction were obtained. The hot-wire signals were sampled at 100 Hz with a recording length of 20 s using a personal computer. Measurement points in the y -axis direction were taken at 1 mm intervals for the boundary layer and wake and at 2 mm intervals for the main flow. The measurements on the y -axis were executed at 5 stations at $x = -100, 4.5, 45, 90$ and 205 mm for the smoothly convergent channel and at $x = -100, 4.5, 45, 90$ and 240 mm for the linearly convergent and parallel channels. On the other hand, the velocities on the z -axis were obtained at stations at $x = 45$ and 90 mm. The measurement uncertainty of the data was 4% for U and 6% for u_{rms} .

3. RESULTS AND DISCUSSION

To verify the effectiveness of the visualization method and to confirm the formation of a turbulent boundary layer on a partition plate, preliminary experiments were executed for a parallel channel. Representative results are shown in Fig. 8. The photographs of the flow in the boundary layer in Fig. 8, were taken from the side and top, where the smoke wire was set in the z' -direction in front of the leading edge. From Fig. 8, one can see that the flow separates at the leading edge, then reattaches and immediately changes into a wavelike flow with a long wavelength, in which the massive smoke produced gradually becomes larger. Near $x' = 300$ mm, a street of large-scale, periodic, transverse vortices with a wavelength of approximately 110 mm is clearly formed. The photographs show that a fully developed turbulent boundary layer [20] is formed on the latter half of the partition plate.

Furthermore, the distributions of the mean velocity and turbulent intensity were examined at the section with $x = -100$ mm ($x' = 400$ mm) before the start of the convergent section. The results are shown in Fig. 9, in which h_0 is the distance between the plate and the channel wall. The results demonstrate that the boundary layer on the plate has a velocity distribution satisfying the 1/7 power law and is about 16 mm thick. On the other hand, a transition boundary layer with a thickness of about 10 mm exists on the channel wall.

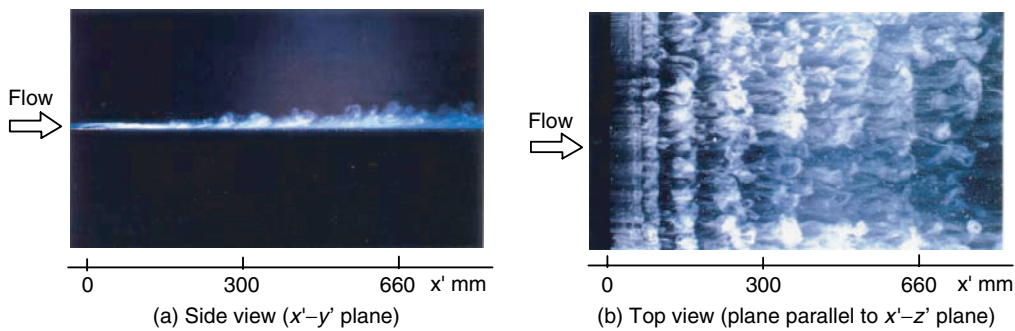


Figure 8. Boundary layer on partition plate ($U_o = 2.0$ m/s).

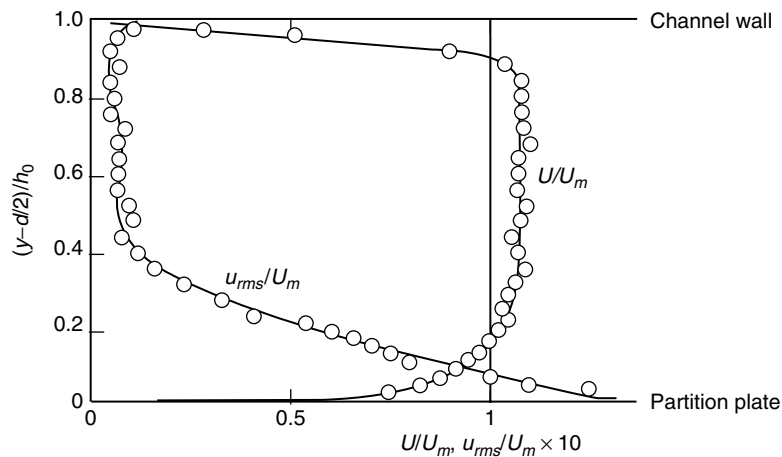


Figure 9. Distributions of mean velocity and turbulence intensity at $x = -100$ mm ($x' = 400$ mm).

3.1. Visualization of Flow Pattern

Photographs of the wake downstream of the trailing edge of the plate inserted in the parallel channel are shown in Fig. 10. To obtain the side view shown in Fig. 10(a), the smoke wire was set at $x = 1$ and $y = 0$ mm, immediately behind the trailing edge. On the other hand, to obtain the top view in Fig. 10(b), the wire was stretched at $x = 2.5$ and $y = 0$ mm. The Reynolds number of the flow, defined as $U_m d/\nu$, is about 10^3 , where U_m is the cross-sectional average velocity in the channel with the plate. This value almost corresponds to that of a headbox of a practical papermaking machine. Illustrations of the boundary layer on the plate are omitted since the flow exhibits a pattern similar to that in Fig. 8, regardless of the shape of the trailing edge and the convergence of the channel, except in the vicinity of the trailing edge (refer to Figs. 12 and 13). In the following, we focus on the flow patterns from the neighborhood of the trailing edge to the wake.

In all cases, the formation of a Karman's vortex street is clearly recognized. Although the wake approximately exhibits periodic, unsteady-flow behavior, the pattern depends on the shape of the trailing edge. In particular, for the rectangular shape, the separated vortex is easily generated at the edge, and one can distinctly observe a Karman's vortex street nearer the trailing edge than that for other shapes. The vortex street is controlled by the channel walls downstream of $x = 150$ mm. Hence, it hardly develops in the y -direction and begins to collapse. For the R-cut shape, the vortices occurring on the side of the R-shape are weak, whereas those observed on the other side predominate in the wake. For the tapered shape, the scale of the vortices generated at the edge is small since the trailing edge has a thickness of $d/10$, which is small compared with that for the rectangular shape. Furthermore, the smoke exhibits linear streaks parallel to the x -axis at $x \leq 50$ mm. Nevertheless, the flow develops with increasing x , resulting in the formation of a vortex street. For the wavy shape, the regularly arranged grooves adjacent to the trailing edge induce longitudinal vortex streets that cause the wake to diffuse. As a result, the wake loses its two-dimensional structure. Hence, the wavy edge does not cause the wake to form a strong, lateral Karman's vortex street.

In illustrating the results for the convergent channels, we demonstrate the dimensionless pressure-gradient coefficient when the above-mentioned wake is accelerated and rectified. Figure 11 shows the acceleration parameter $K = \nu/U_m^2 \cdot (dU_m/dx)$ for the smoothly convergent channel, in which dU_m/dx indicates the change in the cross-sectional average velocity in the stream direction. K increases rapidly from $x = -50$ mm ($x/d = -10$) and reaches a maximum at the trailing edge of the plate ($x = 0$ mm: $x/d = 0$). Its value of 5.2×10^{-5} is notably larger than value of $K \approx 3.5 \times 10^{-6}$ [21, 22] at which the turbulent boundary layer starts to undergo a reverse transition to become laminar. Therefore, the convergence of the channel has a reasonably strong effect on accelerating the boundary layer flow near the trailing edge and wake [17]. In the linearly convergent channel, K is 1.44×10^{-5} .

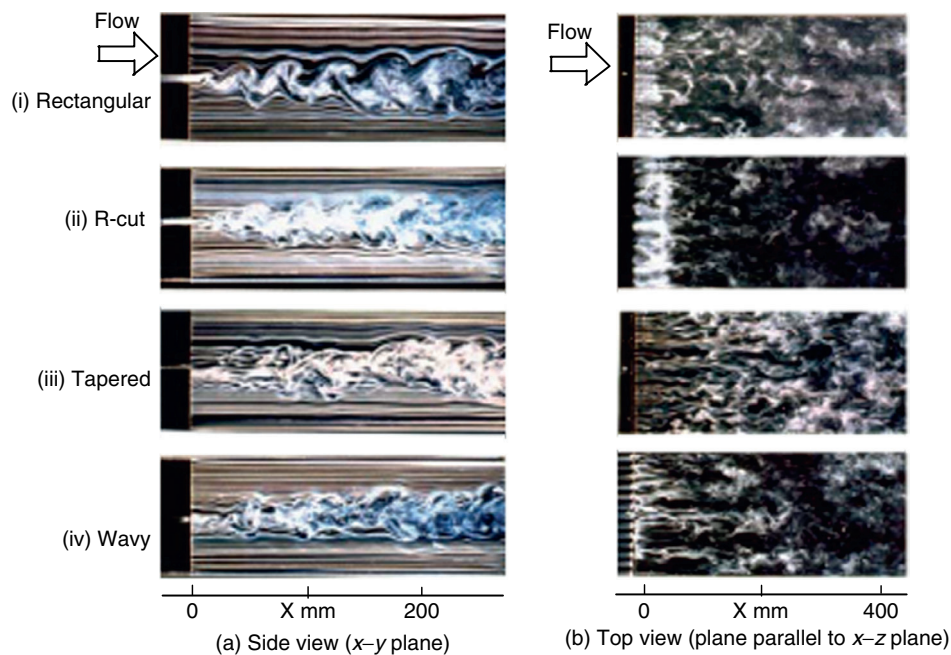


Figure 10. Flow patterns of wake in parallel channel.

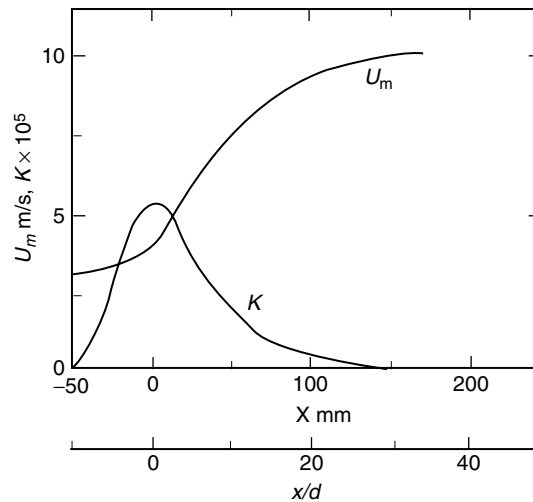


Figure 11. Acceleration parameter K for smoothly convergent channel.

Figures 12 and 13 show streak lines observed in the linearly and smoothly convergent channels, respectively. The photographs were taken in the same way as those taken for the parallel channel. For the linearly convergent channel in Fig. 12, the turbulent boundary layer near the trailing edge on the plate is subjected to accelerative action so that the extension of smoke in the y -direction is suppressed. Furthermore, the rate of increase in the boundary layer thickness in the x -direction is also inhibited. Because of the homogeneous contraction of the entire flow, the wake does not develop into one with an obvious Karman's vortex street, except for the rectangular shape. The flow exhibits wavelike behavior. The width of the Karman's vortex street for the rectangular shape does not markedly change axially owing to the convergence of the channel. Therefore, the flow with the vortex street continues downstream without collapsing. On the other hand, the wavelike behavior temporarily increases its amplitude at $x \approx 60$ and 87 mm for the R-cut and tapered edges, respectively. For the wavy shape, behind the converging part, the fluid flows downstream with wavelike motion with a short wavelength of about 10 mm, similar to the width of the wake.

For the smoothly convergent channel in Fig. 13, the converging effect is extremely strong near the trailing edge of the plate. The wake reduces the number of velocity defects, as will be shown later in Fig. 16. In addition, the wavelike motion weakens owing to the restraint of the converging walls. Thus,

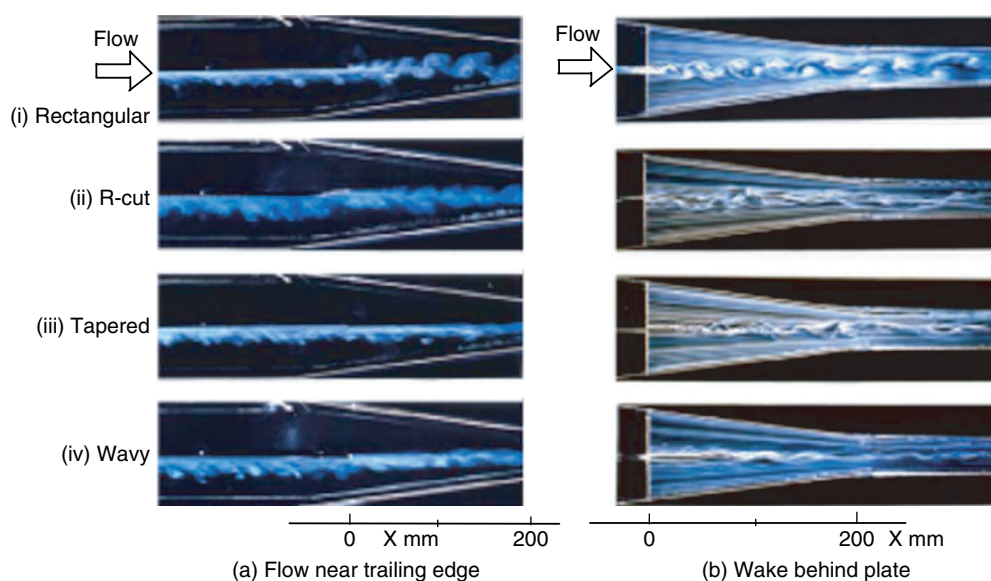


Figure 12. Flow patterns in linearly convergent channel (side view: x - y plane).

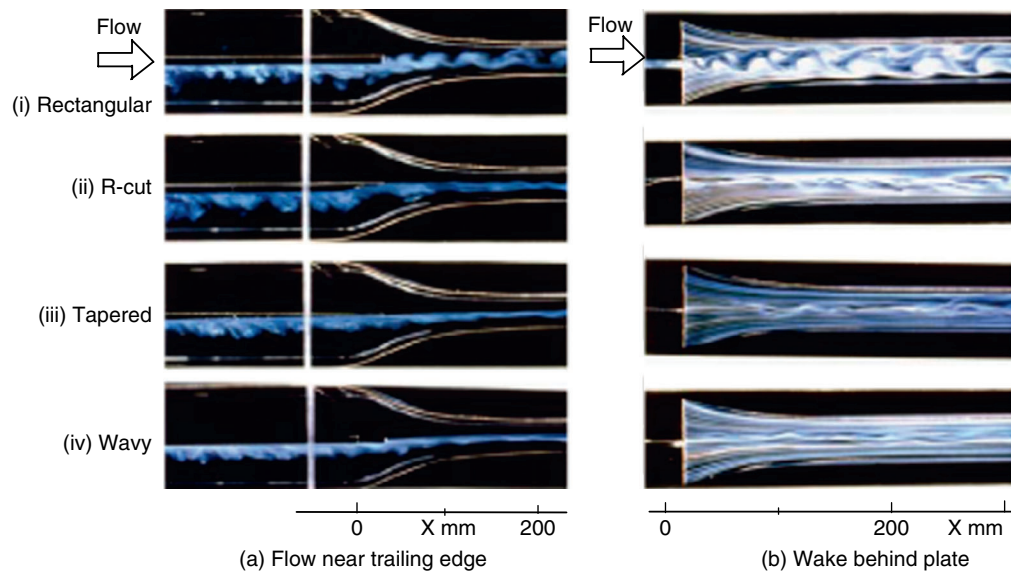


Figure 13. Flow patterns in smoothly convergent channel (side view: x - y plane).

the vortices that separate at the trailing edge do not develop into a flow with discrete vortex streets, even for the rectangular shape, since the convection velocity increases rapidly. Moreover, for the other plates, the wavelike motion observed in the linearly convergent channel is also controlled. This shows that the development of wakes and the generation of vortex streets are considerably restrained.

From the visualization discussed above, we can summarize our findings as follows: i) it is difficult to restrain the generation of a vortex street observed behind a trailing edge, such as the edge with a rectangular shape, by the use of a convergent channel; ii) a smoothly convergent channel has a higher rectifying effect on a wake than the other channels because the acceleration parameter is large near the trailing edge; iii) for both tapered and wavy edges, in particular, there are significant effects promoting the reduction and rectification of a wake in the convergent channels.

Furthermore, for practical use, it is important for the headbox to be used to its full potential by placing the trailing edge at an appropriate position in the convergent channel. That is, it is necessary to adopt a partition plate whose trailing edge produces hardly any turbulence, such as a plate with a tapered or wavy edge. In addition, the thickness of the turbulent boundary layer must be reduced by the contraction and acceleration of the fluid upstream of the trailing edge. Thus, when streams separated by the partition plate smoothly flow together behind the trailing edge of the plate, a uniform velocity profile and the attenuation of turbulence can be expected. On the other hand, for the rectangular shape, although we attempted to obtain a uniform velocity profile by employing a convergent channel, the accelerated flow field resulted in streams that were more strongly separated at the trailing edge. Therefore, a rectifying effect cannot be anticipated.

3.2. Mean Velocity and Turbulence Intensity

Using the results of the above flow observation, the velocity was measured to further quantitatively examine the effects of the shape of the trailing edge and the convergence of the channel. Velocity was measured by hot-wire anemometry with an I-type probe. Trailing edges with rectangular, tapered and wavy shapes were investigated here. Figure 14 shows profiles of the mean velocity U and turbulence intensity u_{rms} on the z -axis, in the central plane of $y = 0$ mm, in the linearly convergent channel. At $x/d = 9$ ($x = 45$ mm), the mean velocity for the tapered edge has a profile with a small undulation. For the wavy edge, on the other hand, U exhibits a profile with a sawtooth-like waveform, of which the teeth correspond to half intervals of the pitch of the wavy shape. However, the mean velocity at $x/d = 18$ ($x = 90$ mm) shifts to a profile with an undulation of about twice the pitch.

The changes in the flow characteristics of the wake along the x -axis are shown in Figs. 15 and 16. In these figures, the turbulence intensity u_{rms} and mean velocity U_c on the centerline of the channel, i.e., the x -axis, are displayed, respectively. Here, u_{rms} is divided by the cross-sectional average velocity U_0

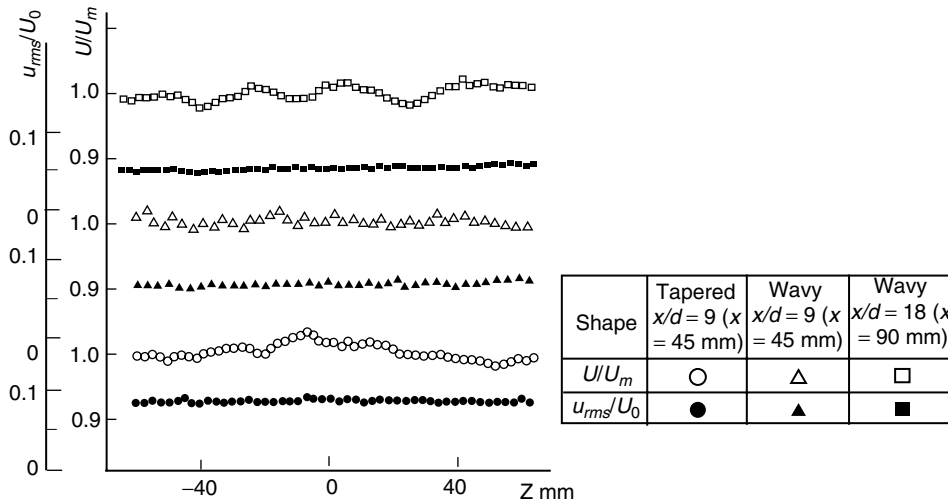


Figure 14. Distributions of mean velocity and turbulence intensity at center of wake in linearly convergent channel.

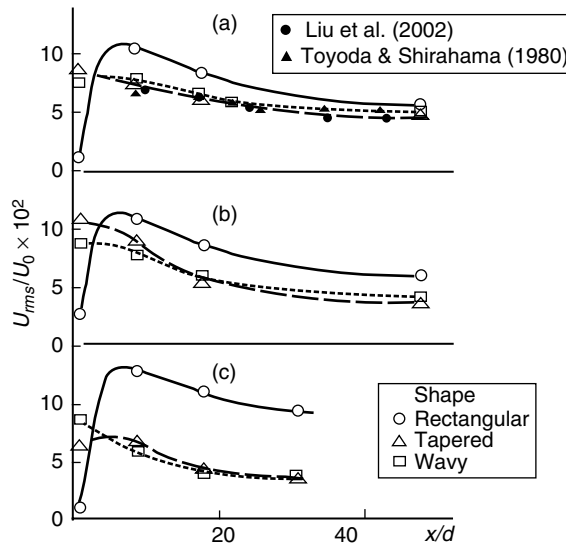


Figure 15. Turbulence intensity u_{rms} on x -axis. (a) Paralell channel, (b) Linearly convergent channel, (c) Smoothly convergent channel.

before the partition plate. Also, U_c is nondimensionalized using the local main-flow velocity U_e in each plane. These quantities are schematically described in Fig. 16. In Figs. 15(a) and 16(a), which show results for the parallel channel, the data of Toyoda and Shirahama [14] and Liu et al. [15] are also illustrated. Toyoda and Shirahama [14] and Liu et al. [15] used 1- and 17.5-mm-thick plates with tapered angles of 1.5 and 2.2°, respectively.

First, we give a general discussion of the characteristics of the parallel channel in Figs. 15(a) and 16(a). For the rectangular shape, vortices of plate thickness order that are separated at the corners of the trailing edge are formed at $0 < x/d \leq 1.2$ ($0 < x \leq 6$ mm) in the shear layer. Hence, the velocity U_c at $x/d = 0.9$ ($x = 4.5$ mm) takes a negative value with a magnitude of about one-tenth of the velocity U_e , and the turbulence intensity is also low. However, slightly further downstream, the flow is accelerated, causing it to turn in the x -direction. Then, the turbulence intensity rapidly increases to its maximum at $x/d \approx 6$ ($x \approx 30$ mm), where a Karman’s vortex street develops. Subsequently, it decreases along the x -axis. On the other hand, for the tapered and wavy shapes, the separated shear layer is so weak that the flow immediately behind the edge is enhanced in the x -direction without flowing

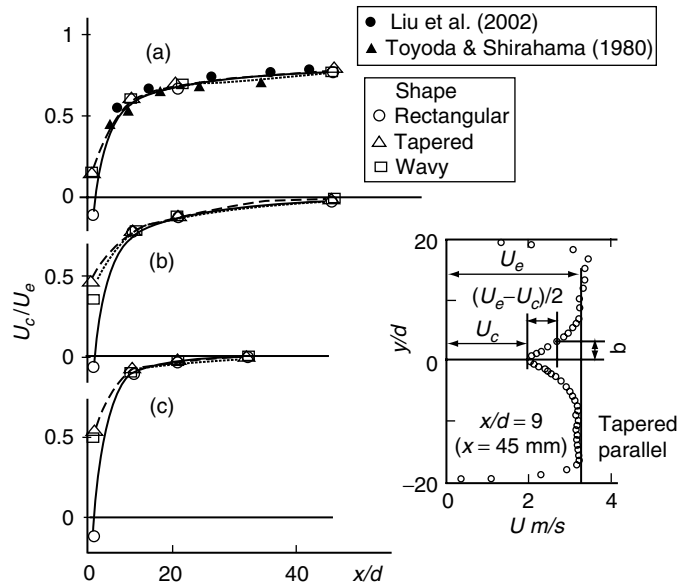


Figure 16. Change in number of velocity defects along x -axis. (a) Parallel channel, (b) Linearly convergent channel, (c) Smoothly convergent channel.

backward. This is because the thicknesses of the trailing edge with the tapered and wavy shapes are 0.3 and 0.5 mm, respectively, which are small. The turbulence intensities for the two shapes are almost equal, and they gradually decrease from 8% near the trailing edges. Downstream of $x/d = 48$ ($x = 240$ mm), where the velocity was measured, there is no significant difference in turbulence intensity between the two shapes and the rectangular shape, as can be seen in Fig. 15(a). In addition, the turbulence intensities at $x/d = 9$ ($x = 45$ mm) for the tapered and wavy shapes are about three-quarters that for the rectangular shape. The reason for the lower turbulence intensity of the tapered shape is that the separated shear layer is weak. For the wavy shape, the flows towards the troughs in its waveform interfere with the wake so that the vortices separated at the trailing edge become weak and the formation of a lateral vortex street is inhibited. As a whole, the characteristics of u_{rms} and U_c along the x -axis for the tapered and wavy shapes agree with those of past data [14, 15] for tapered shapes.

Figure 17 shows the half width b of the wake. As shown in Fig. 17(a), for the parallel channel, there is no effect of the trailing-edge shape on the half width b of the wake. $2b$ increases

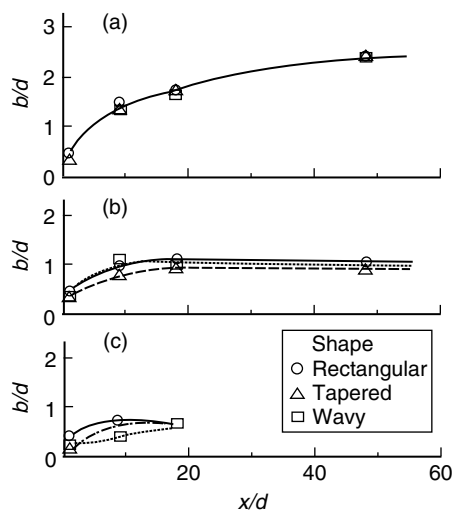


Figure 17. Change in half width of wake along x -axis. (a) Parallel channel, (b) Linearly convergent channel, (c) Smoothly convergent channel.

approximately in proportion to $x^{1/2}$ from d of about 5 mm, since the region with the velocity defect near the trailing edge becomes approximately as thick as the plate. However, the wake is controlled by the walls from $x/d \approx 30$ ($x \approx 150$ mm), gradually reducing its expansion ratio.

Next, we discuss the effect of the convergence of the channel on the wake characteristics. When the channel converges so that the flow contracts, the number of velocity defects is reduced, resulting in a flatter velocity profile. This causes the turbulence intensity to decrease and the flow to be rectified. Furthermore, in the linearly convergent channel, the wake does not extend downstream of $x/d \approx 20$ ($x \approx 100$ mm). For the smoothly convergent channel, on the other hand, the flow loses its feature as a wake since the centerline velocity on the x -axis almost recovers to the local main-flow velocity.

We next shift our attention to the effect of the shape of the trailing edge. For the wavy shape, the dependency of the change in turbulence intensity on the convergence of the channel is comparatively small. For the tapered shape in the smoothly convergent channel, the turbulence intensity is maximum near $x/d = 6$ ($x = 30$ mm) and decreases thereafter, since a strong and highly separated shear layer is produced by the rapid acceleration of the fluid. In addition, the velocity defect of the wake in the smoothly convergent channel almost disappears at $x/d \approx 6$ ($x \approx 30$ mm). Nevertheless, for the rectangular shape, the turbulence intensity in the smoothly convergent channel becomes higher than that in the parallel channel. That is, the rectifying effect of the smoothly convergent channel is counterproductive. The reason for this is as follows. When the acceleration is very large, the vortex separated at the trailing edge of the rectangular shape intensifies and the half width also decreases. Therefore, a highly sheared layer is formed near the channel axis so that a new turbulence is produced.

In an actual papermaking machine, it is desirable to improve the surface properties of paper such that the distributions of average velocity and turbulence intensity are uniform on the y -axis. Moreover, the pulp liquid, i.e., the raw material should be sent from the headbox to the wire part while being accelerated to a certain degree. Thus, we introduce the following quantities as indices that indicate the uniformities of average velocity and turbulence intensity.

$$E_U = \frac{1}{2hU_m} \int_{-h}^h |U - U_m| dy \quad (1)$$

$$E_{rms} = \frac{1}{2hu_{rms,m}} \int_{-h}^h |u_{rms} - u_{rms,m}| dy \quad (2)$$

Here, $h(x)$ is the distance from the x -axis to the channel wall and $u_{rms,m}$ is the cross-sectional average of u_{rms} . The smaller the values of E_U and E_{rms} , the higher the uniformity.

The results for the smoothly convergent channel obtained using Eqs. (1) and (2) are shown in Fig. 18. The uniformity of the average velocity is high for the tapered and wavy shapes. Furthermore, it is

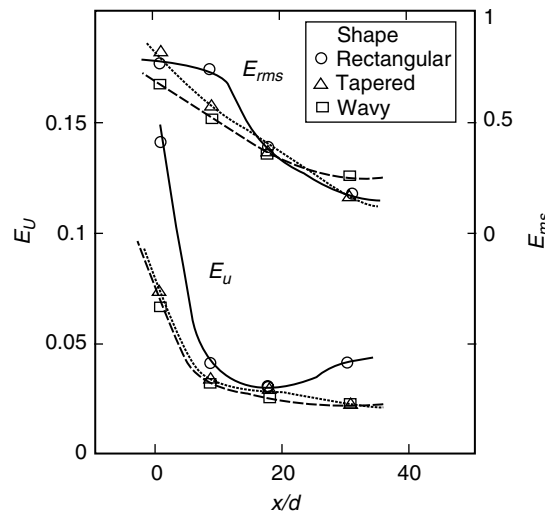


Figure 18. Uniformities of mean velocity and turbulence intensity for smoothly convergent channel.

confirmed that the tapered shape is efficient in terms of achieving uniform turbulence intensity.

4. CONCLUSIONS

Visualization experiments using a smoke-wire method and hot-wire velocity measurement were performed for a flow in a modeled headbox of a papermaking machine. The effects of a convergent channel on the wake behind the partition plate, where a turbulent boundary layer is formed, were investigated. The principal achievements and results of this study are summarized as follows.

- (1) A method of controlling the wake behind the partition plate was developed by adjusting the configurations of the channel and trailing edges, and a scheme for improving the channel in the headbox was obtained.
- (2) Rectification through a convergent channel is effective in achieving a uniform average velocity distribution and in reducing the turbulence intensity. However, for the rectangular shape, the effect of the convergent channel is reduced by half since the vortex separated at the trailing edge develops into a periodic Karman's vortex street, and a rather strong turbulence is produced.
- (3) For the partition plate inserted into the dispersion part of the headbox, it is preferable for the trailing edge to have a tapered configuration. Furthermore, it is advisable to also use a convergent channel.
- (4) Upon applying the results of this study to an actual papermaking machine, a trailing edge with a wavy shape should be used because it is necessary to further improve the dispersion of pulp fibers.

ACKNOWLEDGEMENTS

The authors would like to thank Dr. M. Sugihara and Mr. A. Izawa of Mitsubishi Heavy Industries, Ltd., for helpful discussions. This work was supported in part by JSPS KAKENHI (Grant Numbers 20560173 and 23560212).

REFERENCES

- [1] Makino, T., Takeguchi, N., Eguchi, A. and Tajimi, T., "Development of Concept IV-MH Headbox," *Japan Tappi Journal*, Vol. 48, No. 1 (1994), pp. 42–51 (in Japanese).
- [2] Iijima, H., "The Application of High Speed Paper Making Technology," *Japan Tappi Journal*, Vol. 57, No. 4 (2003), pp. 481–488 (in Japanese).
- [3] Sato, M., "The Latest Headboxes for Board and Packaging Grades," *Japan Tappi Journal*, Vol. 58, No. 12 (2004), pp. 1675–1684 (in Japanese).
- [4] Whalley, R. and Ebrahimi, M., "Optimum Control of a Paper Making Machine Headbox," *Applied Mathematical Modelling*, Vol. 26 (2002), pp. 665–679.
- [5] Linnala, M., Ruotsalainen, H., Madetoja, E., Savolainen, J. and Hämäläinen, J., "Dynamic Simulation and Optimization of an SC Papermaking Line – Illustrated with Case Studies," *Nordic Pulp and Paper Research Journal*, Vol. 25, No. 2 (2010), pp. 213–220.
- [6] Hämäläinen, J., Madetoja, E. and Ruotsalainen H., "Simulation-based Optimization and Decision Support for Conflicting Objectives in Papermaking," *Nordic Pulp and Paper Research Journal*, Vol. 25, No. 3 (2010), pp. 405–410.
- [7] Carlsson, A., Söderberg, L. D. and Lundell, F., "Fibre Orientation Measurements near a Headbox Wall," *Nordic Pulp and Paper Research Journal*, Vol. 25, No. 2 (2010), pp. 204–212.
- [8] Hämäläinen, J., Mäkinen, R. A. E. and Tarvainen P., "Optimal Design of Paper Machine Headboxes," *International Journal for Numerical Methods in Fluids*, Vol. 34 (2000), pp. 685–700.
- [9] Olson, J. A., Friggard, I., Chan, C. and Hämäläinen, J., "Modeling a Turbulent Fibre Suspension Flowing in a Planar Contraction: The One-dimensional Headbox," *International Journal of Multiphase Flow*, Vol. 30 (2004), pp. 51–66.
- [10] Hämäläinen, J. and Makinen R. A. E., "Optimal Control of a Turbulent Fibre Suspension Flowing in a Planar Contraction," *Communication in Numerical Methods in Engineering*, Vol. 22 (2006), pp. 567–575.
- [11] Tani, I. ed., "Progress in Fluid Mechanics (Boundary Layer)," (1984), p. 1, Maruzen (in Japanese).
- [12] Toyoda, K. and Hirayama, N., "Turbulent Wake Flow near the Trailing Edge of a Flat Plate, Part 1: Incompressible Flow," *Transactions of the Japan Society of Mechanical Engineers*, Vol. 39, No. 326 (1973), pp. 3021-3028 (in Japanese).

- [13] Prabhu, A. and Narasimha, R., "Turbulent Non-equilibrium Wakes," *Journal of Fluid Mechanics*, Vol. 54, Part 1 (1972), pp. 19–38.
- [14] Toyoda, K. and Shirahama, Y., "A Study of Turbulent Wake Flow near a Flat Plate, 3rd Report: Effects of Pressure Gradients," *Transactions of the Japan Society of Mechanical Engineers*, Vol. 46 (B), No. 406 (1980), pp. 1046–1054 (in Japanese).
- [15] Liu, X., Thomas, F. O. and Nelson, R. C., "An Experimental Investigation of the Planar Turbulent Wake in Constant Pressure Gradient," *Physics of Fluids*, Vol. 14, No. 8 (2002), pp. 2817–2839.
- [16] Liu, X. and Thomas, F. O., "Measurement of the Turbulent Kinetic Energy Budget of a Planar Wake Flow in Pressure Gradients," *Experiments in Fluids*, Vol. 37 (2004), pp. 469–482.
- [17] Parsheh, M. and Dahlkild, A. A., "Evolution of Flat-plate Wakes in Sink Flow," *Journal of Fluid Mechanics*, Vol. 626 (2009), pp. 241–262.
- [18] Lane, J. C. and Loehrke, R. I., "Leading Edge Separation from a Blunt Plate at Low Reynolds Numbers," *Transactions of the ASME, Journal of Fluids Engineering*, Vol. 102 (1980), pp. 494–496.
- [19] Tani, I., Kobashi, Y. and Sato, H. ed., "*Experimental Method of Fluid Mechanics*," (1977), p. 254, Iwanami (in Japanese).
- [20] Taneda, S., "The Structure of Turbulent Boundary Layers," *Nagare*, Vol. 1 (1982), pp. 29–35 (in Japanese).
- [21] Morretti, P. M. and Kays, W. M., "Heat Transfer to Turbulent Boundary Layer with Varying Free-stream Velocity and Varying Surface Temperature (An Experimental Study)," *International Journal of Heat and Mass Transfer*, Vol. 8 (1965), pp. 1187–1202.
- [22] Kline, S. J., Reynolds, W. C., Schraub, F. A. and Runstadler, P. W., "The Structure of Turbulent Boundary Layer," *Journal of Fluid Mechanics*, Vol. 30 (1967), pp. 741–773.